Title

A study of thermal pressurization and potential for hydro-fracturing associated with nuclear waste disposal in argillaceous claystone

Authors

Xu, Hao
Rutqvist, Jonny
Birkholzer, Jens

Publication Date

2020-12-01

DOI

10.1016/j.ijrmms.2020.104536

Peer reviewed

International Journal of Rock Mechanics & Mining Sciences 136 (2020) 104536

Contents lists available at ScienceDirect

International Journal of Rock Mechanics and Mining Sciences

journal homepage: http://www.elsevier.com/locate/ijrmms

A study of thermal pressurization and potential for hydro-fracturing associated with nuclear waste disposal in argillaceous claystone

Hao Xu, Jonny Rutqvist *, Jens Birkholzer

Energy Geosciences Division, Earth & Environmental Sciences Area, Lawrence Berkeley, National Laboratory, Berkeley, CA, USA

ARTICLE INFO

Keywords:
Thermal pressurization
Fracturing
Callovo-oxfordian claystone
THM
Nuclear waste disposal

ABSTRACT

We present coupled Thermo–Hydro–Mechanical (THM) modeling of geologic nuclear waste disposal in argillaceous claystone, focusing on thermally-induced pressure changes and the potential for such pressure changes to induce hydro-fracturing. To investigate this possibility, we first conduct a three-dimensional repository scale model, with host rock properties, repository design, and nuclear waste decay heat functions derived from the French concept of geologic disposal in argillaceous claystone. The model simulations show that the highest potential for hydro-fracturing occurs between emplacement micro-tunnels (cells) at the center rather than at the edge of the repository. We further investigate the use of a two-dimensional single cell model as a simpler surrogate for a full three-dimensional model. Our results reveal that such geometric simplification is reasonably accurate for modeling coupled THM processes at the center of the repository, though it overestimates the likelihood for hydro-fracturing and substantially overpredicts ground surface uplift. A parameter study shows the importance of adjacent higher permeability geological layers that play a significant role in dissipating overpressure in the host rock layer. Finally, the study shows the importance of the spacing between emplacement tunnels, which if too short results in a higher fluid pressure and a strongly increased potential for hydro-fracturing. Overall, the study suggests, the limiting factor in the thermal management and design of a repository is not necessarily the maximum temperature in the engineered barrier system near the waste packages, but rather the more modest host rock temperature between emplacement tunnels, due to the potential for thermal damage.

1. Introduction

Argillaceous claystone formations have been studied as a potential host rock for nuclear waste disposal. This includes Callovo-Oxfordian (COx) claystone in France,[1,2] Boom clay in Belgium,[3,4] and Opalinus clay in Switzerland,[5,6] while argillaceous clay or shale is also considered as an option in the U.S. and Canada.[7,8] Argillaceous claystone has several favorable properties for nuclear waste isolation, including low permeability, good sorption capacity, limited natural fracturing and capacity for self-sealing.[7] However, the low thermal conductivity may lead to higher temperatures and thermal gradients in response to the emplacement of heat-producing nuclear waste. This together with a low rock permeability tends to induce strongly coupled Thermo-Hydro-Mechanical (THM) processes that are important to investigate for performance assessment.[2,9] Thermal pressurization is a prominent coupled process that occurs in low permeability claystone as a result of the difference between the thermal expansion coefficients of the fluid and the claystone.[9–11] If exceeding the minimal principal stress, the increase in the pore pressure could induce hydro-fracturing or might induce shear on existing fractures.[11,12]

In this paper we study these strongly coupled processes at the repository scale. The work is performed as part of the DECOVALEX (DEvelopment of COupled models and their VALidation against EXperiments) project, an international research and model comparison collaboration for understanding and modeling of coupled thermo-hydro-mechanical-chemical processes in geological systems.[13] The DECOVALEX-2019 phase was running from 2016 through 2019, and this study falls under Task E related to upscaling from lab scale to repository scale using data from heater experiments performed at the Meuse/Haute-Marne (MHM) Underground Research Laboratory (URL), in Bure, France.[14,15] The first sub-task of DECOVALEX-2019 Task E consisted of model validation against *in situ* COx heating experiments at the MHM URL, involving thermal pressurization.[14,16] This model validation is an important step and provides confidence in the model and

* Corresponding author.
E-mail address: Jrutqvist@lbl.gov (J. Rutqvist).

https://doi.org/10.1016/j.ijrmms.2020.104536
Received 14 May 2020; Received in revised form 20 October 2020; Accepted 21 October 2020
Available online 9 November 2020

model simulations related to thermal pressurization at the repository scale.

The modeling study presented in this paper is related to the final subtask of DECOVALEX-2019 Task E, which focuses on simulating the coupled THM processes at the repository scale. The task considers the repository design envisioned by the French national radioactive waste management agency (ANDRA) for nuclear waste disposal in COx claystone. According to this design, the canisters holding high-level nuclear waste will be emplaced in a set of parallel micro-tunnels (or cells) of 0.80 m diameter and 150 m length as part of the blue zone (Zone C) shown in Fig. 1[17] In this study, a three-dimensional (3D) THM model is constructed that includes over a hundred nuclear waste emplacement cells (micro-tunnels), a system of access tunnels which in our simulations either will be left open or will be backfilled after repository closure, and a detailed representation of vertical geological layering. The host rock properties, repository design, and decay heat emitted from the emplaced nuclear waste are provided by ANDRA, with host rock properties derived from the site investigations at the MHM URL.[14] Starting with the complex 3D model, we investigate the potential of geometric model simplifications by applying a symmetric two-dimensional (2D) single cell model, a type of model simplification that is commonly used for these kinds of computationally demanding coupled processes simulations.[18,19] The 2D model is also utilized for relevant parameter sensitivity studies.

In the following Section 2, we introduce the fundamental equations describing coupled THM processes in porous deformable rock as well as the numerical simulator applied in this study. In Section 3, we proceed with the 3D repository modeling of thermal pressurization and fracture potential. In Section 4, we investigate the use of a symmetric 2D single cell model and this model is then used in Section 5 for parametric studies on the effects of host rock permeability and cell spacing. We end with a discussion of the results in the light of previous studies and their relevance to thermal management and repository design, and conclude by identifying our main findings and future work.

2. Theoretical background and TOUGH-FLAC simulator

The numerical simulator used here solves THM coupled processes in rocks based on the theory of thermo-poro-elasticity.[16] The governing equation for geomechanics is based on the quasi-static assumption, written as

$$\mathrm{Div}\boldsymbol{\sigma} + \rho_b \boldsymbol{g} = 0, \tag{1}$$

where Div is the divergence operator; $\boldsymbol{\sigma}$ is the total stress tensor; ρ_b is the bulk density; and $\boldsymbol{g}$ is the gravity vector. The stress in the solid skeleton can be expressed as

$$d\boldsymbol{\sigma} = \mathbb{C} : d\varepsilon - \boldsymbol{b} dp - \mathbb{C} : \boldsymbol{\alpha} dT, \tag{2}$$

where $\mathbb{C}$ is the tensor of skeleton tangent elastic stiffness modulus; ε is the strain tensor; $\boldsymbol{b}$ is the Biot's tangent tensor; p is the pore pressure; $\boldsymbol{\alpha}$ is the tensor of skeleton tangent thermal dilation coefficients; and T is the absolute temperature.

The governing equations for fluid and heat flow are derived from conservation laws. The governing equation for fluid flow is

$$\boldsymbol{b} : d\varepsilon + \frac{1}{M} dp - 3\alpha_m dT + \nabla \cdot \boldsymbol{f}^f = 0, \tag{3}$$

$$\boldsymbol{f}^f = -\frac{\boldsymbol{K}}{\mu_f}\left(\nabla p - \rho_f \boldsymbol{g}\right), \tag{4}$$

where $\frac{1}{M} = \frac{1}{N} + \frac{\varphi}{K_f}$; N is the Biot's tangent modulus linking the pressure variation and the porosity variation; φ is the porosity; K_f is the fluid tangent bulk modulus; $\alpha_m = \alpha_\varphi + \varphi\alpha_f$; $3\alpha_\varphi$ is the volumetric thermal dilation coefficient related to the porosity; $3\alpha_f$ is the fluid tangent coefficient of volumetric thermal dilation; $\boldsymbol{f}^f$ is the Darcy flux; $\boldsymbol{K}$ is the permeability tensor; μ_f is the fluid viscosity; and ρ_f is the fluid density.

The governing equation for heat flow is

$$\frac{dM^h}{dt} - \nabla \cdot \left(\lambda_t \nabla T - h_f \rho_f \boldsymbol{f}^f\right) = 0, \tag{5}$$

$$M^h = (1-\varphi)\rho_s C_s T + \varphi \rho_f C_f T, \tag{6}$$

where M^h is the heat storage term; ρ_s is the density of the solid skeleton; C_s and C_f are the specific heats of the solid skeleton and fluid, respectively; λ_t is the thermal conductivity; and h_f is the specific enthalpy of the fluid.

The above governing equations are solved using a sequentially coupled finite differential simulator - TOUGH-FLAC,[20] which links the multi-phase flow transport simulator - TOUGH2[21] and the geomechanical simulator - FLAC3D.[22] A sequential technique is used[20]

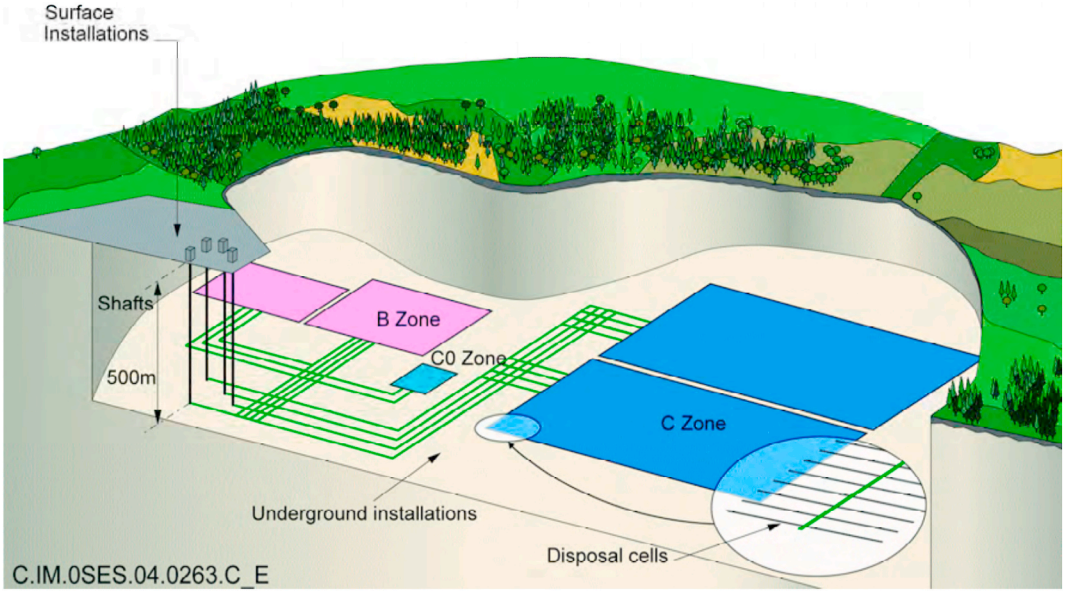

Fig. 1. General architecture of a potential disposal in the Callovo-Oxfordian formation.[17]

through a carefully derived pore-volume coupling, or porosity correction.[23] The TOUGH-FLAC simulator was recently verified and validated for modeling coupled THM processes in argillaceous clay, with properties corresponding to the COx claystone.[16] This includes validations for modeling of thermal pressurization in the COx claystone at the MHM URL. The validated model is used here for simulation of thermal pressurization and associated stress changes at the repository scale.

3. Repository scale 3D THM model

This section presents the development and results of the repository scale 3D THM model. We first introduce the model, including geometry and mesh discretization in Section 3.1, initial and boundary conditions in Section 3.2, and material parameters in Section 3.3. This is followed by simulation results showing the evolution and distribution of temperature, pressure and stress in Sections 3.4 and 3.5. Finally, for the 3D THM model, an investigation of the approach for modeling the access-drift backfill is presented in Section 3.6.

3.1. Geometry and mesh discretization

The domain of the repository model is represented by a quarter symmetry of a full scale repository with the dimensions 2000 m × 1500 m × 1000 m as shown in Fig. 2. Eight geological layers are defined vertically in the geological model and these are considered with the properties listed in Table 3. The COx formation is vertically divided into three unit layers: the Clay unit (UA), the Transition unit (UT), and the Silty Carbonate-Rich unit (USC), defined in terms of mineralogical composition.[15] The cells for disposal of nuclear waste canisters are designed to be at a depth of 560 m underground in the UA2-UA3 formation. The emplacement cells, access and connection tunnels are explicitly represented in the 3D repository model. The cylindrical cells are simplified by cuboid elements in the model. According to the repository design provided by ANDRA as part of the DECOVALEX-2019 Task E, 28 cells are placed on each side of the access tunnel with a cell spacing of 52.3 m between each other. In terms of the numerical discretization, the 3D model contains 343,669 tetrahedrons and 59,431 nodes/vertexes in total. The maximum element size in the UA2-UA3 layer is 50 m at the outer edge of the model, while the minimum size is 0.3 m near the emplacement cells.

Modeling results are presented as (1) contour plots showing the spatial distribution across the entire repository horizon at selected times, and (2) time evolution plots at selected points in the interior and at the edge of the repository (Fig. 2). The points we use to plot the evolutions are marked as A_1, B_1, C_1, and B_2 in Fig. 2; their coordinates and output variables are listed in Table 1. One of the critical outputs presented is the vertical effective stress, which is an important indicator of the potential for hydraulic fracturing due to thermal pressurization.

3.2. Initial and boundary conditions

Based on the site description provided by ANDRA, initial and boundary THM conditions are applied to the model. The initial temperature is assumed to be linearly dependent on the depth with constant values of 7.7 °C at the top and 37.7 °C at a depth of 1000 m at the bottom of the model. Based on ANDRA's best estimates of the stress field at the site, the initial pore pressure is set as 0 MPa at the ground surface and varies with depth in accordance with a gradient of 0.01 MPa/m, representing hydrostatic conditions. An initial stress distribution is applied with a depth gradient of 0.024 MPa/m for the vertical stress and minimum horizontal stress, and with a gradient of 0.032 MPa/m for the maximum horizontal stress. The highest temperature is designed to be

Table 1
Points for Output numerical results.

Points	Positions	Output Quantity
A_1	2 m to the right of the 14th cell center.	Temperature, Pore Pressure, Total/ Effective Stress.
B_1	In the middle between the 14th and 15th cells.	Temperature, Pore Pressure, Total/ Effective Stress.
C_1	Above B_1 on the top surface.	Displacement.
B_2	In the middle between the 27th and 28th cells.	Temperature, Pore Pressure, Total/ Effective Stress.

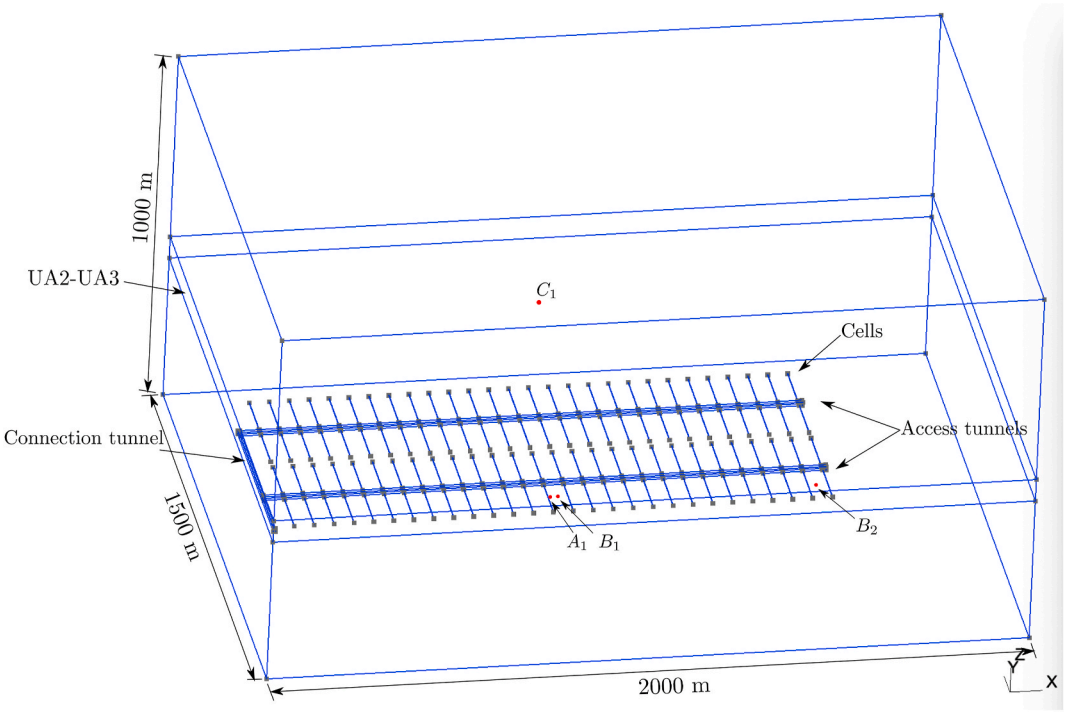

Fig. 2. Simulation domain and model output points.

about 90 °C, which is below the boiling point. Thus, all rock formations are assumed fully saturated and remain saturated during the whole heating process. It is noted that in the current model we do not consider ventilation or gas generation.

Our simulation starts with the excavation of the access and connection tunnels followed by ten years of drainage into the open tunnels. Thereafter the drilling of 112 (28 × 4) cells (horizontal micro-tunnels) is simulated to take place instantly, followed by another two years of drainage, after which the emplacement of waste canisters into the cells occurs, again simultaneously. We do not consider any excavation damage zone around the tunnels or cells. The reference date at zero years corresponds to the starting point of the cell excavations.

The decay heat power from waste canisters emplaced in the cells starts at 146 W/m, then decays following the curve shown in Fig. 3.

In terms of model boundary conditions, the top surface of the model domain refers to the ground surface, and is free to move, while the bottom surface is constrained to have zero vertical displacement. The vertical symmetry planes are fixed with zero normal displacements, while the far-field vertical boundaries have fixed stress values varying linearly with depth according to the aforementioned initial stress gradients. Boundary conditions for the cells and the access tunnels during the three processing stages were defined by ANDRA as part of the DECOVALEX-2019 task and are listed in Table 2[15] The assumption of atmospheric pressure in the access tunnel for 10,000 years as defined in Table 2 might imply that these tunnels remain open and are not completely water filled for 10,000 years. In our modeling we investigate an alternative to this assumption by simulating a case of the access tunnels being naturally resaturated due to inflow from the surrounding rock.

3.3. Material parameters

Material parameters for the COx claystone and other units above and below the host rock unit were provided by ANDRA as described in Plúa et al.[15,24,25] Property estimates are based on characterization in the MHM URL and data from several deep boreholes that were drilled in the planned disposal area. Horizontal bedding in the COx formation are present from the sedimentary origin of the rock unit. This leads to a slight anisotropy of most rock properties, particularity in terms of permeability, thermal diffusivity and mechanical parameters. The bedding parallel stiffness, the permeability, and the thermal conductivity of the COx are all greater than their corresponding bedding perpendicular values, respectively (anisotropy ratio ranging between 1.2 and 3.0). The mean values for THM parameters of each unit are used

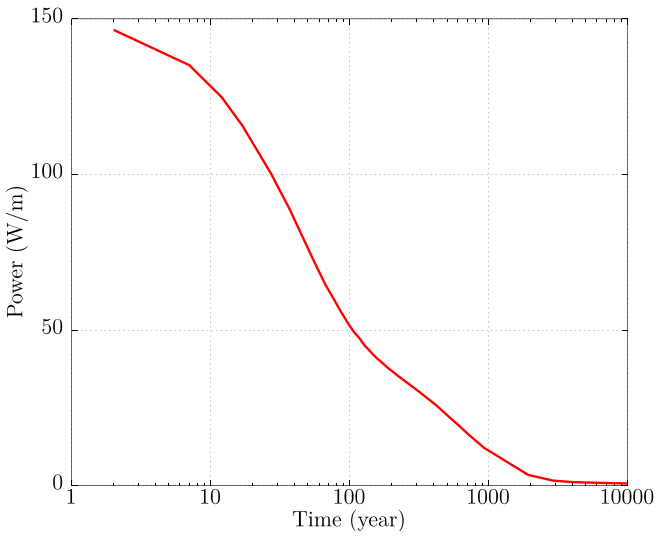

Fig. 3. Decay heat power per meter along each cell applied in the model.

Table 2
Boundary conditions on the cell and tunnel walls.[15]

		Cells	Access tunnel
−10 – 0 years	T	24.5 °C	24.5 °C
	H	Hydrostatic pore pressure.	Atmospheric pressure.
	M	Considered as UA2-UA3 with lithostatic stress.	Free surface.
0–2 years	T	Initial temperature.	Initial temperature.
	H	Atmospheric pressure.	Atmospheric pressure.
	M	Free surface.	Free surface.
2–10,000 years	T	Heat power	Initial temperature but can change.
	H	No flux.	Atmospheric pressure.
	M	Free surface.	Free surface.

in the simulation, and they are listed in Table 3. Water properties in the TOUGH-FLAC simulation are calculated from the steam table equations,[26] which is standard in TOUGH2. One enhancement for TOUGH2 is that we have implemented the equations accounting for anisotropic thermal conductivity. The model used here is based on thermo-poro-elasticity, which is explained in Section 2.

3.4. Results

Fig. 4 presents the model predictions in terms of temperature, pore pressure, displacement, and stress. As mentioned before, time = 0 is when the assumed instantaneous excavation of the emplacement cells occurs. Starting from the initial value of 24.5 °C at this depth level, the temperature at point A_1 near the cell peaks at about 57 °C after 25 years, whereas the peak temperature at point B_1 in the midway distance between cells is about 42 °C (Fig. 4(a)) after 500 years. At about 2000 years, the temperature evolutions at points A_1 and B_1 merge, indicating a uniform temperature in the repository layer, follow the same evolution, and thereafter decrease towards the ambient temperature till the end of the simulation.

Fig. 5 displays the spatial distribution of temperature at different times. As the figure shows, at 20 years, the temperature is highest (above 55 °C) in very close vicinity to the 112 cells, and very little temperature increase is seen in the host rock between the cells (Fig. 5(a)). Then, at 50 years, the high temperature zone surrounding the cells expands, and the temperature between the cells rises to about 40–50 °C. Even later (100–500 years), as a result of the decaying heat power, the peak temperatures near the cells decrease from their peak values, which eventually leads to a more evenly distributed temperature in the whole emplacement zone.

The pore pressure changes at points A_1 and B_1 are quite different (Fig. 4(b)). Since point A_1 is close to the cell, the early time drainage into the cell (after excavation) results in an initial reduction of pore pressure at this location. After the waste is emplaced, the pore pressure increases rapidly to reach 9.5 MPa at around 5 years, and it peaks at 10.2 MPa, above the initial hydrostatic pressure of 5.6 MPa (Fig. 4(b)). This rapid pressure increase is caused by thermal pressurization of the pore water which has limited capability to move away from the cells due to the low permeability of the COx claystone. In contrast, the pore pressure at point B_1 (in the center between cells) only slightly decreases for about 1.5 years after the waste emplacement, but then increases to a peak of 10.5 MPa at 35 years. However, the access tunnels and connection tunnel still have very low pore pressure since atmospheric pressure is imposed at these locations in the model. After 35 years, the fluid pressure at both locations begins to dissipate, and almost follows the same path for up to 2000 years when hydrostatic equilibrium is re-established.

Fig. 6 presents the spatial distribution of pore pressure at 20, 50, 100 and 500 years. As this figure shows, the pore pressures surrounding the cells increase above 9 MPa at 20 years (Fig. 6(a)), and then the high pore pressure from the temperature increase induce the water flows horizontally between the cells, resulting in an evenly distributed high pore

Table 3
THM parameters of different rock formations used in the repository scale model.[15]

Rocks		E_v	E_h	ν	b	n	K_v	K_h	ρ	λ_v	λ_h	α_s	C_p	Depth
		GPa	GPa		–	–	m^2	m^2	kg/m^3	W/m/K	W/m/K	1/°C	J/kg/K	m
Barrois Limestone		3.6	3.6	0.3	0.6	0.13	1.00E-19	1.00E-19	2450	1.1	1.54	2.20E-05	1024	0–103.4
Kimmeridgian		3.6	3.6	0.3	0.6	0.13	1.00E-19	1.00E-19	2450	1.1	1.54	2.20E-05	1024	103.4–211.4
Carbonated Oxfordian		30.	30	0.3	0.6	0.13	1.00E-16	1.00E-16	2470	2.3	2.3	4.50E-06	925	211.4–488
Callovo-Oxfordian	USC	12.8	19.2	0.3	0.6	0.15	1.87E-20	5.61E-20	2480	1.79	1.79	1.75E-05	978	488–517.4
	UT	8.5	12.75	0.3	0.6	0.173	1.87E-20	5.61E-20	2450	1.47	2.205	1.75E-05	978	517.4–532.6
	UA2-UA3	7.	10.5	0.3	0.6	0.193	1.87E-20	5.61E-20	2430	1.31	1.965	1.75E-05	978	532.6–595.8
	UA1	12.5	18.75	0.3	0.6	0.164	1.87E-20	5.61E-20	2460	1.63	2.445	1.75E-05	978	595.8–635
Dogger		30.	30	0.3	0.6	0.1	1.00E-18	1.00E-18	2470	2.3	2.3	4.50E-06	925	635–1000

pressure between cells at 50 years. Later, the pore pressure dissipates to hydrostatic pressure as a result of the decline in temperature and drainage.

In terms of sensitivity to the boundary conditions, we also checked the temperature and pore pressure at the right and back far edges of the domain at the same depth as points A_1 and B_1, and found that the temperature changed by only 2 °C, and the pore pressure changed by about 0.4 MPa. With these small fluctuations, the domain is ensured to be large enough without significant impact of boundary effects.

Fig. 4(c) shows the vertical displacement change at point C_1 at the top of the model domain (ground surface). The heat emanating from the canister generates large thermal expansion in the UA2-UA3 clay formation, leading to a ground surface heave of 88 mm. The peak surface uplift occurs at around 1700 year, which is delayed compared to the repository peak temperature as surface uplift is due to the cumulative thermal expansion of host rock and overburden, which takes longer to propagate to the ground surface. Later, with contraction and energy dissipation during the cooling period, the surface heave reduces to 20 mm at 100,000 years.

Fig. 4(d) and (e) display the evolution of vertical total and vertical Terzaghi effective stresses at points A_1 and B_1 in the COx claystone. The vertical Terzaghi effective stress is the difference between the vertical total stress and the pore pressure, $\sigma'_{zz} = \sigma_{zz} - p$. Positive stress indicates compressive stress. The evolution of total stress in Fig. 4(d) results from pore pressure changes and thermal stress based on thermo-poro-elasticity. The total stress at point A_1 near the cell drops abruptly at 2 years because of micro-tunnel excavations. However, this decrease reverses shortly thereafter, when the heat emanating from the waste induces thermal expansion, resulting in a gradual increase of compressive stress. The total stress at point A_1 reaches a maximum compressive stress at 10 years and then slowly recovers to its initial static stress value after about 10,000 years. The total compressive stress at point B_1 decreases initially after cell excavation and waste emplacement, but then increases again within 80 years and remains close to a vertical stress equal to the weight of the overburden.

The vertical effective stress evolution at each point follows the associated pore pressure evolution. At point B_1, a substantial effective compressive stress decrease, which reaches a minimum of 3.2 MPa at about 40 years, increases the potential for tensile failure (e.g., approaching $\sigma'_{zz} = 0$). As the figure shows, the reduction of the effective stress is mainly a result of the fluid pressure increase by thermal pressurization. At point A_1, while there is also a thermal pressurization leading to effective stress decrease, the minimal value of the effective stress is 7.2 MPa, which offers a significant safety margin compared with zero stress conditions (or the potential for tensile damage). However, this is an issue that needs to be revisited when different parameters are considered in the design, such as the spatial distance between cells. During later times after 1000 years, the gradual effective stress increase at both points is mainly a result of the cooling contraction.

Fig. 7 displays the vertical effective stress distribution across the repository from 20 years to 500 years. The vertical effective stress shows stronger decreases in the middle between cells at 20 years (Fig. 7(a)), but then the areas of stronger decreases expand horizontally towards the cells at 50 years. Later, with pore pressure dissipation, the effective stress recovers to its initial state.

3.5. Comparison between different locations

With this detailed 3D model, we can also track the simulation results at other locations. Here we choose point B_2, which is a middle point between the 27th and 28th cells near the right edge of the emplacement zone. In terms of the relative location between two cells, point B_2 has a similar position as point B_1. However, we recall that point B_1 is closer to the center of the repository while point B_2 is between two micro-tunnels at the very end of the repository footprint. Therefore, point B_2 is subjected to different THM conditions than B_1.

Fig. 8 presents the simulated results at point B_2 in comparison to B_1, to show the effects of being located at the edge of the repository. As Fig. 8 illustrates, the evolution of temperature, pore pressure, and vertical effective stress at B_2 follow the same path as B_1 up to 10 years. Because B_2 is close to a non-heating zone at the edge of the repository, the thermal energy and fluid pressure can dissipate towards the unheated rock beyond the repository, resulting in an earlier temperature decrease compared to B_1 (after 50 years compared to 200 years, respectively), and an earlier pore pressure reduction. The compressive stress between the 27th and 28th cells also increases due to different confinement from the unheated rock. As Fig. 8(c) shows, the total vertical compressive stress at B_2 increases to 15.2 MPa, resulting in a higher effective stress than at B_1. This result indicates that the rock volumes at the edge of the repository have a lower potential of tensile fracturing than in the center.

3.6. Backfilled tunnels with bentonite

As an alternative to assuming the access tunnels stay open and provide draining boundary conditions for 10,000 years, here we investigate the case of all access tunnels being backfilled after waste emplacement. We assume that all tunnels are backfilled with a bentonite-crushed rock mixture. The Young's modulus of the backfill is assumed to be 17 MPa, the initial saturation is 65%, and the permeability is assumed to be one order magnitude higher than the host rock in the UA2-UA3 layer. We use a simple relative permeability function, in which all phases are perfectly mobile (i.e. relative permeability for gas and liquid are $k_{rg} = k_{rl} = 1$), and a capillary pressure function, in which the capillary pressure does not depend on the saturation, to account for multiphase flow in the bentonite. The alternative case is marked as "3D, backfilled" in the results presented in Fig. 9.

As Fig. 9 shows, the temperature evolution at points A_1 and B_1 is almost the same for both cases. The pore pressures for both cases also follow the same path until about 200 years after emplacement. After that time, the access tunnels are almost fully saturated with water in the backfilled case, resulting in a slower drainage from the host rock to access tunnels, which causes a higher pore pressure as shown in Fig. 9 (b). Moreover, the final hydrostatic pore pressure in the backfilled case

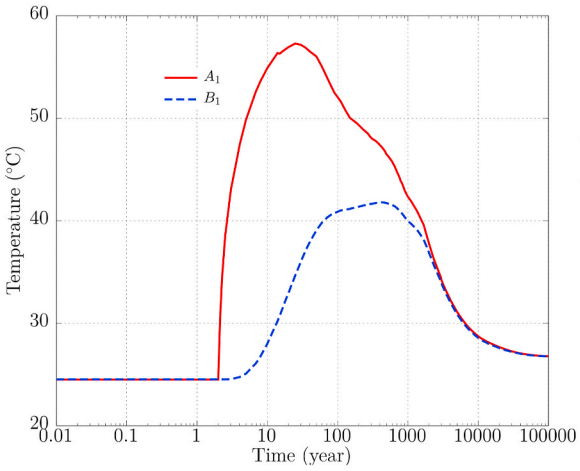

(a) Temperature evolution at A_1 and B_1.

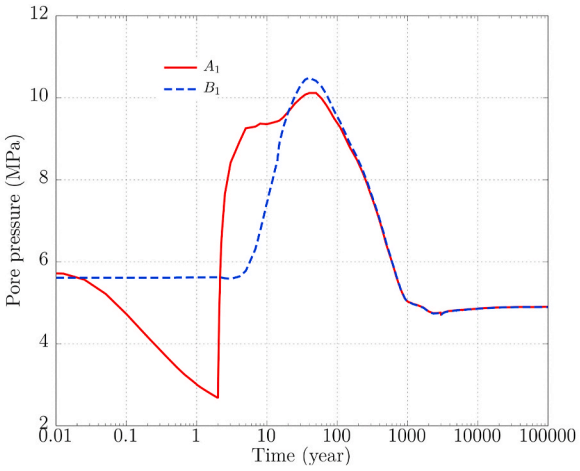

(b) Pore pressure evolution at A_1 and B_1.

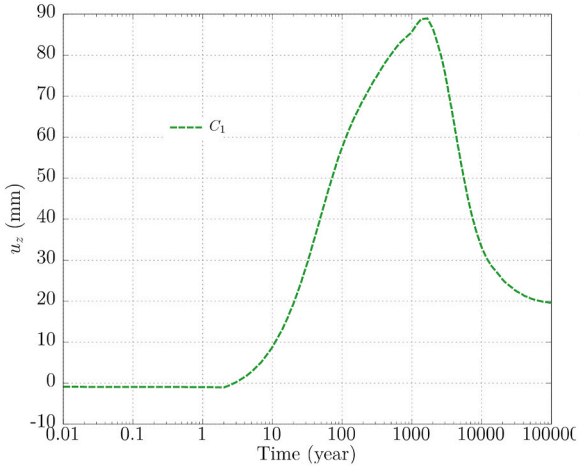

(c) Displacement changes at C_1.

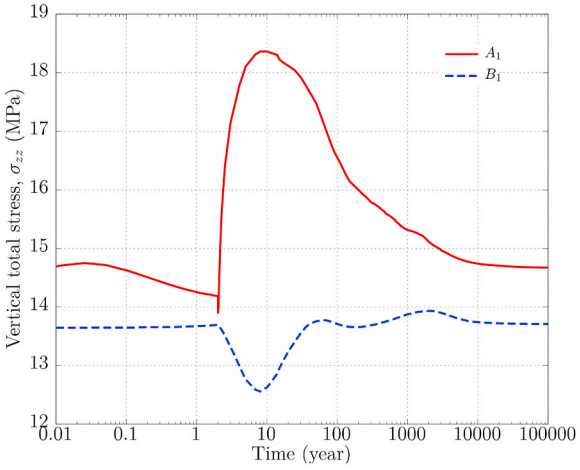

(d) Vertical total stress changes at A_1 and B_1.

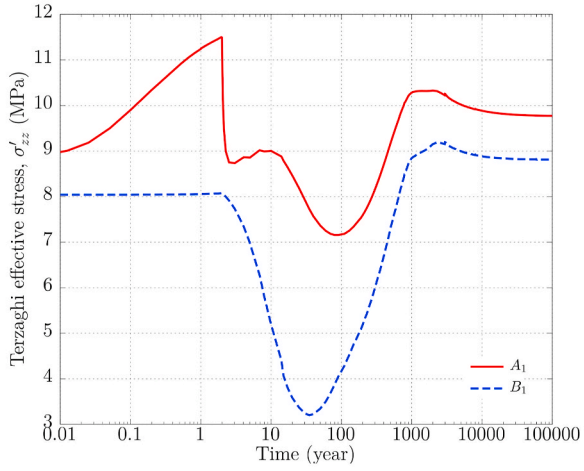

(e) Vertical Terzaghi effective stress changes at A_1 and B_1.

Fig. 4. 3D THM simulation results.

is about 1 MPa higher than the original case which imposes a drainage boundary condition in access tunnels. In the backfilled case, the displacement at the ground surface also diverges after about 200 years when the access tunnels are fully saturated. The peak and final value of vertical displacement both increase due to the expansion from the backfilled material in the tunnels. As Fig. 9(d) suggests, the support from the backfill in the tunnels results in a reduced stress concentration at A_1, but no significant change can be seen at B_1. The new case leads to a lower peak value of vertical effective stress at A_1, while the peak at B_1 is the same as the original case.

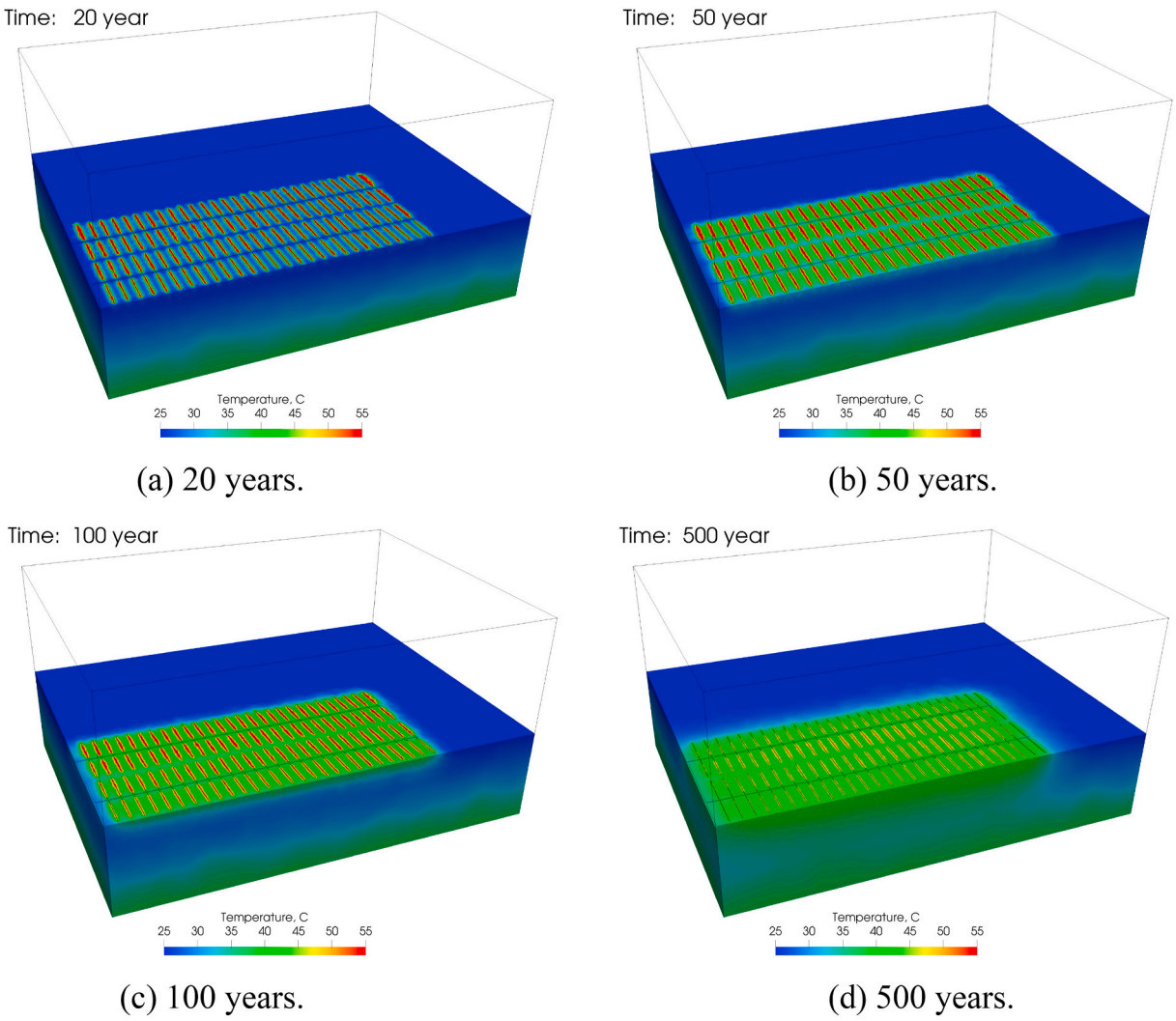

Fig. 5. Temperature distribution in the lower half domain at different times.

4. Simplified 2D single cell model

In order to capture accurately the steep gradients that occur near the micro-cells and tunnels as a result of excavation and emplacement, the model domain needs detailed mesh refinement around these openings. In a full 3D model, this requirement can lead to a very large number of elements which makes the simulations computationally expensive. It is thus no surprise that fully coupled THM simulations of an entire repository have rarely been done. In contrast, researchers frequently choose to adopt simplified 2D model strategies for the problem. In this section, we consider such a 2D model strategy; we select a vertical cross-section perpendicular to the micro-cells and further simplify the geometry by using symmetry assumptions to represent only one cell and the surrounding rock up to the mid-plane between the neighboring cells. This 2D model is under a plane strain condition and, with sufficient refinement near the openings, contains only 15,675 tetrahedrons and 5329 nodes. Note that the 2D model is a single layer of the full 3D model. All x- and y-planes are considered as symmetric planes, and are mechanically constrained with zero normal displacements. The other initial conditions are the same as in the previous 3D model.

The comparisons of the simulation results are presented in Fig. 10 in terms of temperature, pore pressure, displacement, vertical total stress, and vertical effective stress. In the 2D model, point A_1 is 2 m horizontally from the nearest cell, point B_1 is at the right boundary with the same depth as A_1, and C_1 is above B_1 at the top surface. In general, the results of the different models display similar responses but with some differences in magnitude. Both 3D and 2D models exhibit almost the same behavior for temperature up to 4000 years. The slight differences during this period mainly come from the space discretization (mesh generation) and time discretization (time increments controlled by the simulator). The pore pressure evolution for both models also follows a similar path, but for the 3D model, the pressure starts to dissipate earlier and the final value is lower than for the 2D model. Since the 3D model represents all cells with center and edge locations, it allows for more rock volume to dissipate the thermal-induced pressurization, and thus the pore pressure for the 3D model drops earlier than for the 2D model. Fig. 10(c) shows the displacement evolution at point C_1 in both models. The 2D model simulation predicts a much larger ground surface heave of 190 mm, while in the 3D model, the ground surface heave is 88 mm, i.e., less than half of the 2D model. The difference is due to the fact that the 2D model neglects the rigidity against flexural bending of the overburden that is considered in the full 3D model. The 2D model can only expand vertically due to thermal effects, so the whole volumetric expansion contributes to the vertical displacement increase. Thus, the simplified 2D model will strongly overestimate the vertical displacement. For the total stress presented in Fig. 10(d), the 2D model predicts less compression stress at both locations compared to the 3D model. As a result, the vertical effective stress in the 2D model is lower at both locations, as shown in Fig. 10(e). Thus, in terms of evaluating the potential for tensile stresses to evolve and cause damage, the 2D predictions are more

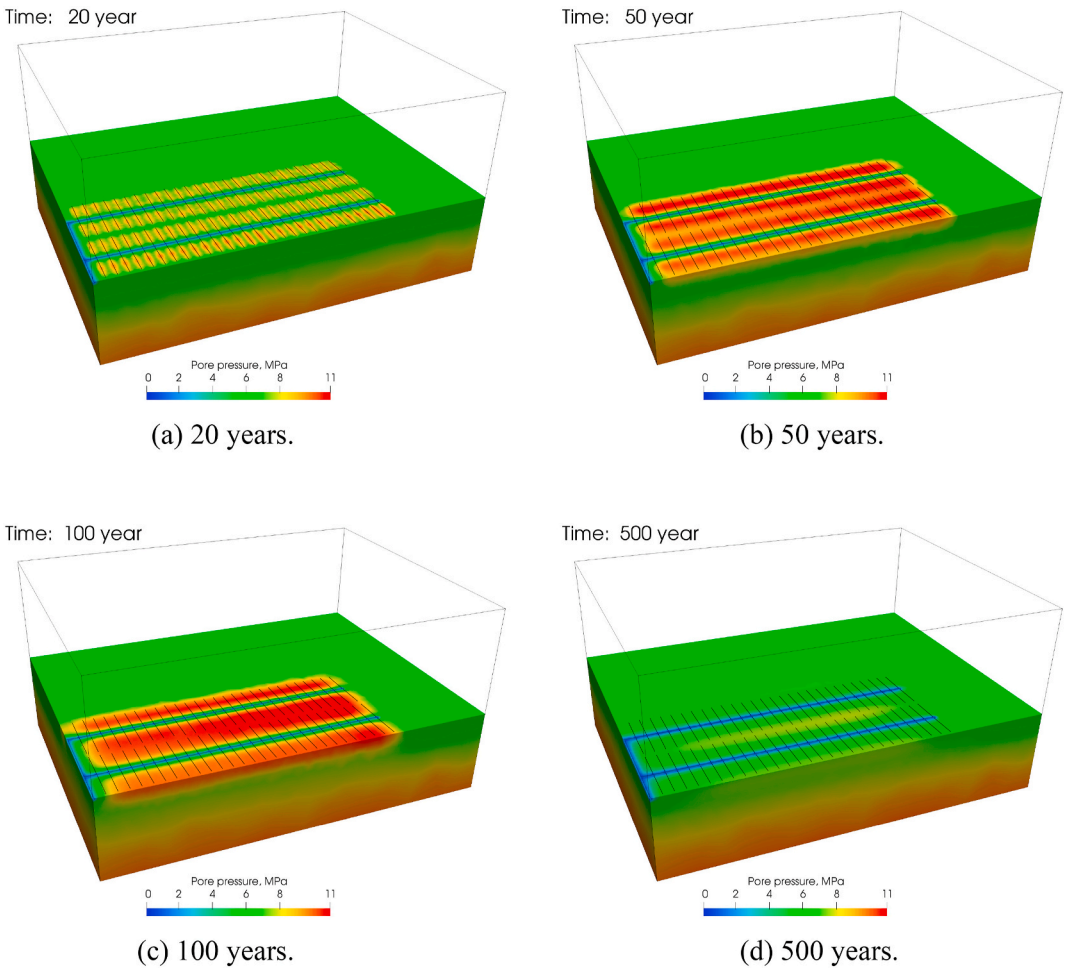

Fig. 6. Pore pressure distribution in the lower half domain at different times.

conservative than the 3D results. We conclude that a 2D representation may be used as an alternative model method to capture the trends of the near-field behavior of COx claystone while avoiding excessive computational expense. However, the magnitudes of displacement and stress are not exact, as Fig. 10(c) to 10(e) illustrate, and this needs to be accounted for when evaluating the 2D simulations. Since a 2D model geometry requires less work and is computationally more efficient than a full 3D model geometry, the advantage of using a 2D model is that we can obtain a quick indication of the likely limiting factors. After that, we can build a 3D model for an accurate result.

5. Parametric study with 2D model

As the previous section explains, a 2D representation provides a reasonable approximation of the rock behavior compared to a full 3D model, in particular when the interest is on evaluation of sensitivity cases where trends are more important than the exact magnitude of the predictions. Therefore, for computational efficiency, we utilize the 2D model to conduct a parametric study on host rock permeability and cell spacing.

5.1. Permeability

In the original 2D model, the COx claystone has a much lower permeability than the layers just above and below. Thus, the pore pressure increases from thermal pressurization in the COx host rock will readily dissipate when reaching these more permeable formations. In this section, we apply the permeability of the COx claystone to all formations, but keep all other parameters the same as before, to investigate the rock behavior and pore pressure evolution when the whole has a low permeability. One additional point D_1, which is 120 m above point B_1 in the COx layer, is used to monitor the pore pressure evolution in that layer.

Fig. 11 provides a comparison of these two permeability cases as predicted with the 2D THM model. The original 2D case is marked with "2D: case 1", while the new case with homogeneous permeability is marked with "2D: case 2". The temperature and vertical total stress at points A_1 and B_1 are essentially the same for both cases, since these two variables are not strongly dependent on permeability. In contrast to the original case, the period of elevated pore pressure at both points A_1 and B_1 lasts much longer in the new case, from a few tens of years to a few thousand years. Clearly, the lower permeability in the entire model domain causes a much slower pressure dissipation away from the repository, not just in the repository horizon but also at point D_1 about 120 m above in the COx, as shown in Fig. 11(f). As a result of that, the minimum of effective stress also lasts longer as Fig. 11(e) shows. Thus, with a lower permeability, the potential for tensile fracturing increases and a higher vertical expansion at C_1 is obtained in Fig. 11(c).

5.2. Cell spacing

Fig. 12 shows the THM evolution for a 2D model with a smaller cell spacing, 35 m, in comparison to the original case with a cell spacing of 52.3 m. As the figure shows, the peak values of temperature and pore pressure both increase strongly when the micro-tunnels for waste emplacement are closer together. The vertical displacement at C_1 does

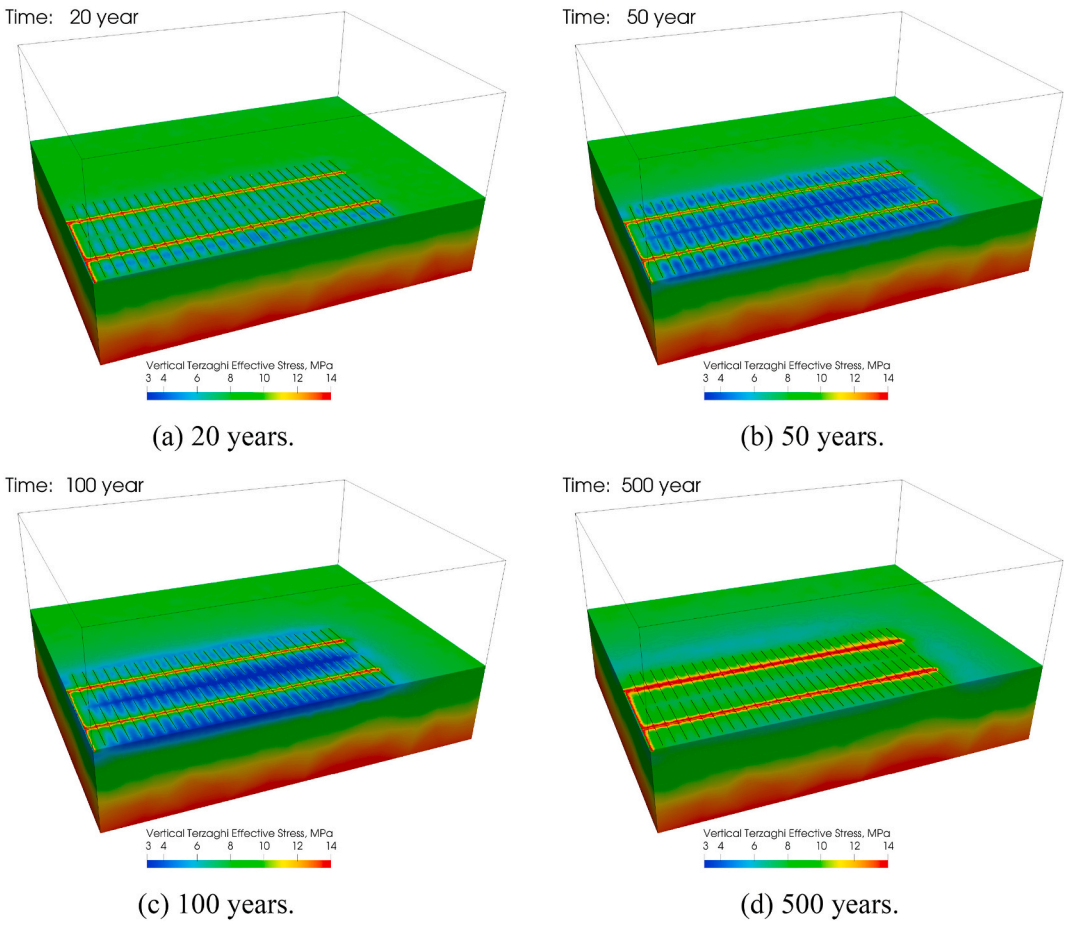

Fig. 7. Vertical Terzaghi effective stress distribution in the lower half domain at different times.

not change much, while the vertical total compressive stress at points A_1 and B_1 reduces by about 0.6 MPa at the peak. This together with the increased pore pressure results in an decrease of vertical effective stress at both locations for the case with smaller distance between cells. In Fig. 12(e), the effective stress at B_1 in the new case drops to about 0 MPa, possibly inducing tensile fracturing. This analysis illustrates the fact that the cell spacing is a critical parameter for the nuclear waste repository design, because if the distance between the micro-tunnels becomes too small tensile fracturing of the COx may occur in the rock midway between two neighboring cells.

6. Discussion

Our simulation study shows that the THM processes occurring as a result of the long-term heating of the host rock have important repository-scale manifestations that should be considered in the repository design.[28] Our results demonstrate the strong impact of thermal pressurization on the repository stress evolution in low permeability argillaceous claystone.[9,28] Interestingly, the impact of thermal pressurization on the repository stress evolution and fracture potential is driven by the average repository host rock temperature, not the maximum temperature experienced near the emplacement tunnels.[9,28] This is also well illustrated in the results of Fig. 12 of this study: at 10 years, a first pressure peak occurs in the near field (point A_1 and red lines in Fig. 12 (b)), which is driven by the sharp increase in near field temperature (point A_1 and red lines in Fig. 12(a)). However, the second pressure peak is much higher, it occurs uniformly at both A_1 and B_1, and it correlates with the average repository temperature evolution (blue lines in Fig. 12 (a) and (b)). This is most apparent when decreasing the distance between the emplacement cells from 52.3 to 35 m. As a result, the second pressure peak becomes so high that the effective stress goes to zero, suggesting that tensile failure is possible. In these two cases, the cell temperature is always around 81 °C, less than the 90 °C which is the maximum temperature limit set by ANDRA for the COx claystone. This illustrates the fact that the longer-term average repository or center emplacement temperature may be the limiting factor in the repository design rather than the near-field temperature that peaks much earlier.

It is relevant to compare simulation results obtained for emplacement in micro-tunnels as envisioned by ANDRA with emplacement in regular-in-drift disposal concepts as modeled in Rutqvist et al.[9] and Rutqvist.[28] Those latter simulations were performed for Opalinus Clay host rock which has similar thermo-poro-elastic properties as the COx claystone; also, a similar spacing between emplacement tunnels was assumed, i.e. about 50 m. However, the decay heat functions are at much higher power in those simulations compared with the function used here in Fig. 3. The impact of the decay heat power is especially apparent for the case of the large-sized nuclear waste canisters considered in Rutqvist[28], where the host rock temperature increases significantly and causes a high potential for hydro-fracturing. Moreover, the simulations in Rutqvist[28] were conducted under the assumption of uniform low permeability of the overburden rock layers. In the results of Fig. 11, we found that the presence of a higher permeability layer just above or below the repository layer has a significant impact on the long-term pressure evolution as it helps dissipate the high overpressure created by thermal pressurization. This illustrates the importance of including the geological layers above and below the repository horizon when conducting repository-scale TMH simulations.

The model simulations also show that a 2D single cell model provides surprisingly accurate predictions of the temperature and pressure evolutions compared to a full 3D repository model. Some differences occur

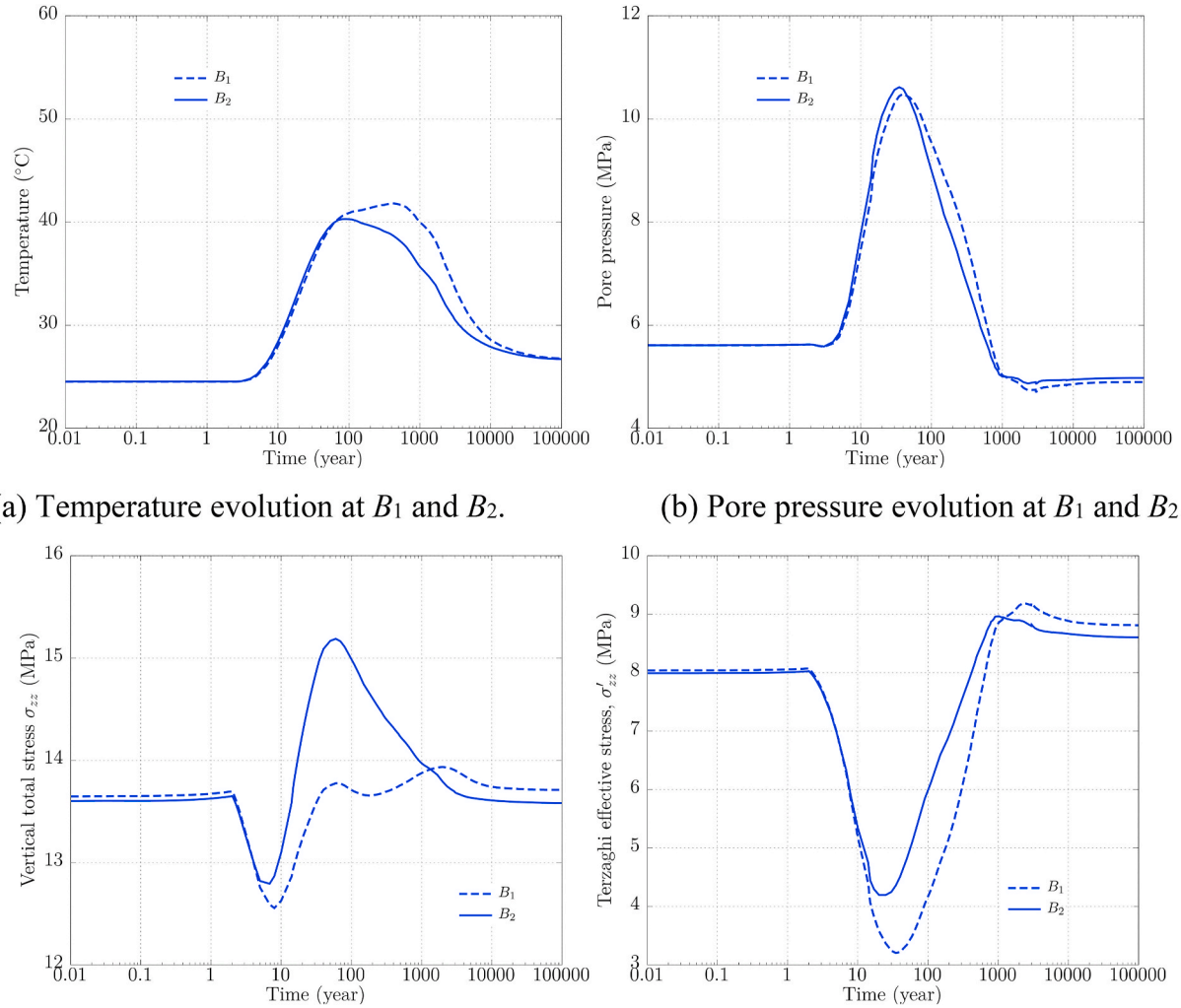

(a) Temperature evolution at B_1 and B_2. (b) Pore pressure evolution at B_1 and B_2.

(c) Vertical total stress changes at B_1 and B_2. (d) Vertical Terzaghi effective stress changes.

Fig. 8. Comparison of THM simulation results for B_1 and B_2.

in the calculation of effective stress and the potential for hydro-fracturing is somewhat overestimated in the 2D single cell model. The reason as previously described is that the 2D model neglects the rigidity to flexural bending of the overburden that is considered in the full 3D model. As it gives conservative estimates for damage potential, the 2D model thus can be used for optimization studies where the objective is to develop repository designs with dense arrangement of emplacement cells but no hydro-fracturing. The 2D model results represent the inner parts of the repository where the temperate and pressure changes are highest. The 3D repository model, in turn, can study the distribution of THM evolution over the entire repository, such as at the edge of the repository, and can also account for sequential tunnel drilling and waste emplacement, which in reality will not occur simultaneously over the entire repository. Notably, here we have proven that coupled THM modeling can be conducted at the repository scale for over 100,000 years.

An important future study would involve THM simulations to calculate what would happen if hydro-fracturing actually occurs. This can be achieved with the current model by adopting elasto-plasticity in the simulations with anisotropic strength properties, as the horizontal fracturing would likely take place along the bedding planes of the COx claystone. Ideally, such simulations would not only involve calculation of hydro-fracture propagation and distribution, but also the potential for long-term sealing and healing of such fractures. Experimental, in-field, and modeling studies on fractures in COx claystone and Opalinus Clay indicate that natural fractures and induced fractures tend to seal hydraulically over time once the pressure has been reduced to below the total normal stress (meaning the normal effective stress becomes compressive) across the fracture.[27,29,30]

7. Conclusions

We have conducted coupled THM modeling of geologic nuclear waste disposal in argillaceous claystone, focusing on thermally-induced pressure changes and the potential for hydro-fracturing at the repository scale. The host rock properties, repository design and nuclear waste decay heat evolution were derived from the French concept of geologic disposal in COx claystone. However, the processes and typical responses can be generalized to a repository hosted in a similar low permeability argillaceous claystone or shale. The following are the main findings from this study:

- The model simulations show that the highest potential for fracturing of the rock occurs at the midpoint between individual emplacement tunnels (rather than in the vicinity of the tunnels) and at the center of the repository (rather than at its edge). The reason is that thermally-induced pore pressure increases are highest at the center of the repository but the stress confinement is low, while some confining

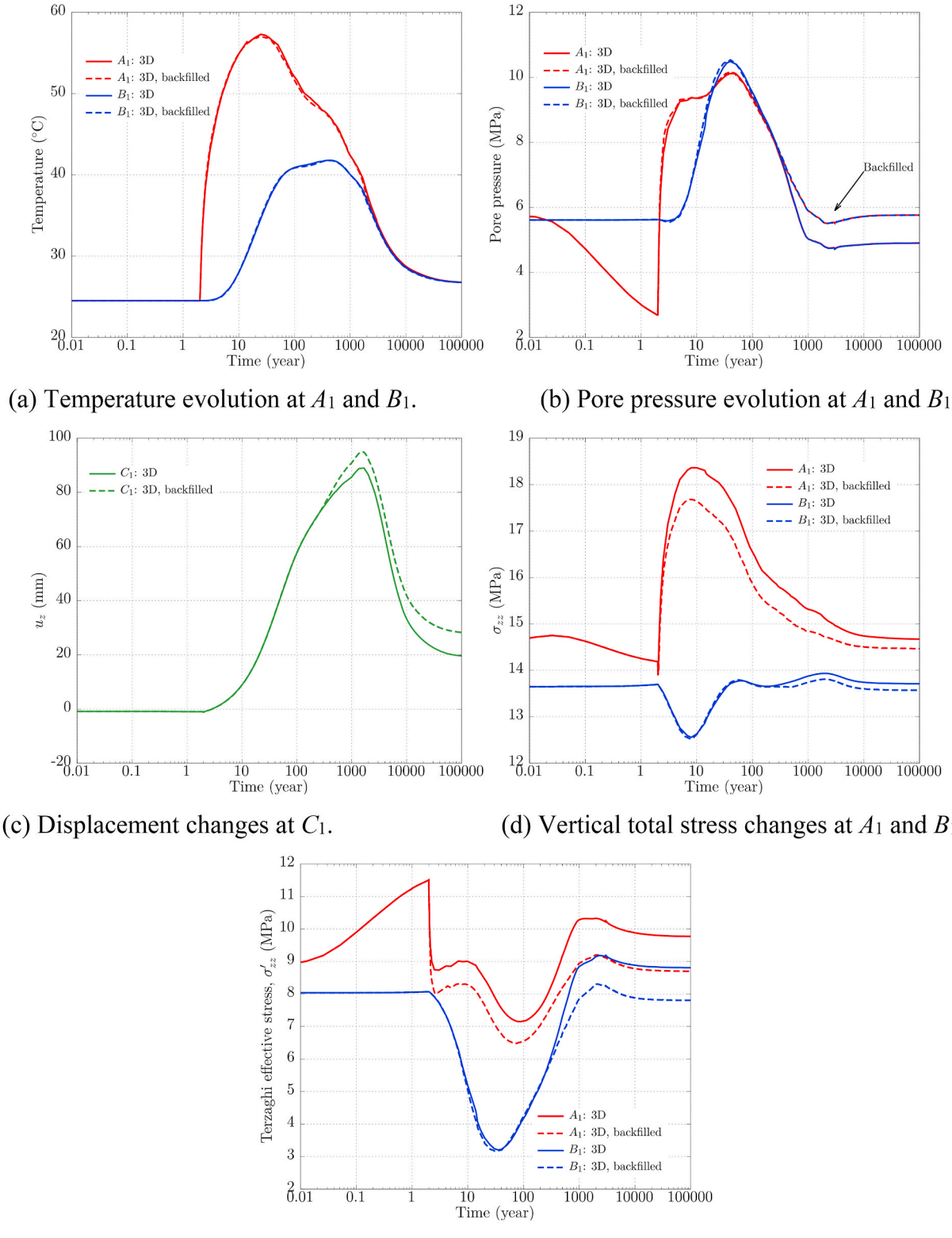

(a) Temperature evolution at A_1 and B_1.

(b) Pore pressure evolution at A_1 and B_1.

(c) Displacement changes at C_1.

(d) Vertical total stress changes at A_1 and B_1.

(e) Vertical Terzaghi effective stress changes at A_1 and B_1.

Fig. 9. Comparison of THM simulation results between the original 3D case and the case with backfilled bentonite in tunnels.

stress increase tends to occur and prevent hydro-fracturing adjacent to emplacement tunnels and at the edge of the repository.

- A simplified 2D model of a single emplacement tunnel predicts the coupled THM processes near the center of the repository reasonably well, though it tends to overestimate the likelihood for hydro-fracturing and significantly overestimates ground surface uplift. Such a 2D model provides a convenient option for studies to investigate the sensitivity to various parameters.
- It is important to include realistic THM properties not only of the repository host rock layer, but also for geological layers above and

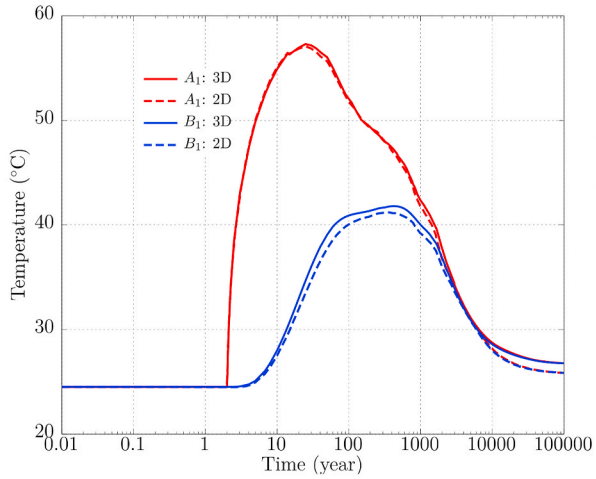

(a) Temperature evolution at A_1 and B_1.

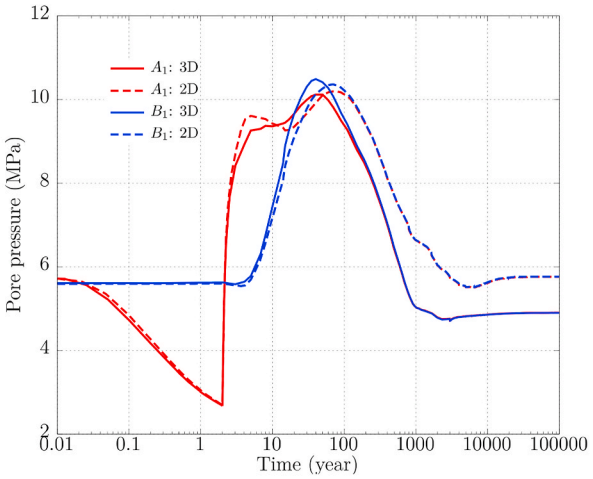

(b) Pore pressure evolution at A_1 and B_1.

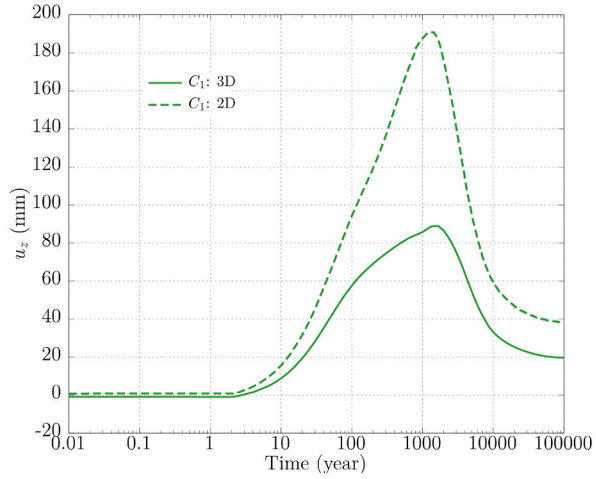

(c) Displacement changes at C_1.

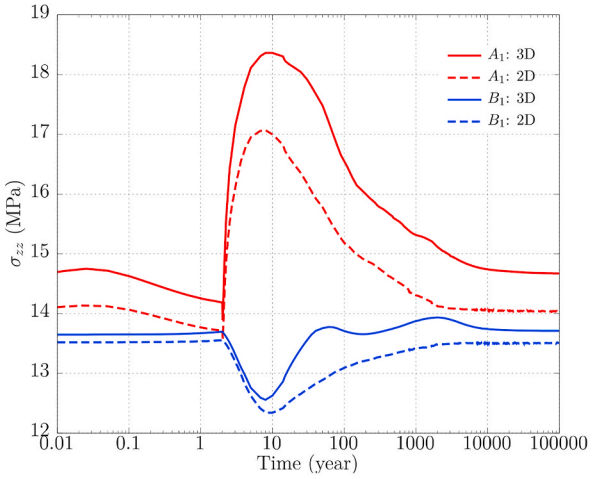

(d) Vertical total stress changes at A_1 and B_1.

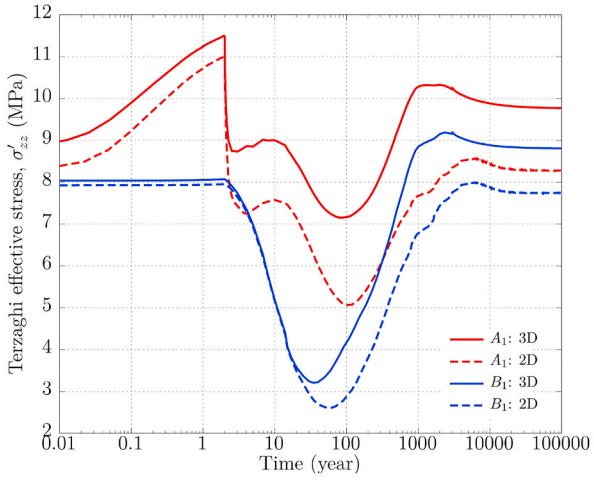

(e) Vertical Terzaghi effective stress changes at A_1 and B_1.

Fig. 10. THM simulation results with 2D and 3D model configurations for comparison.

below. As an example, a larger permeability in these over- and underlying layers helps dissipate thermally-induced overpressure in the host rock layer.

- The spacing between emplacement tunnels is a critical design parameter that affects the host rock temperature evolution and therefore also affects thermal pressurization and the potential for hydro-fracturing.

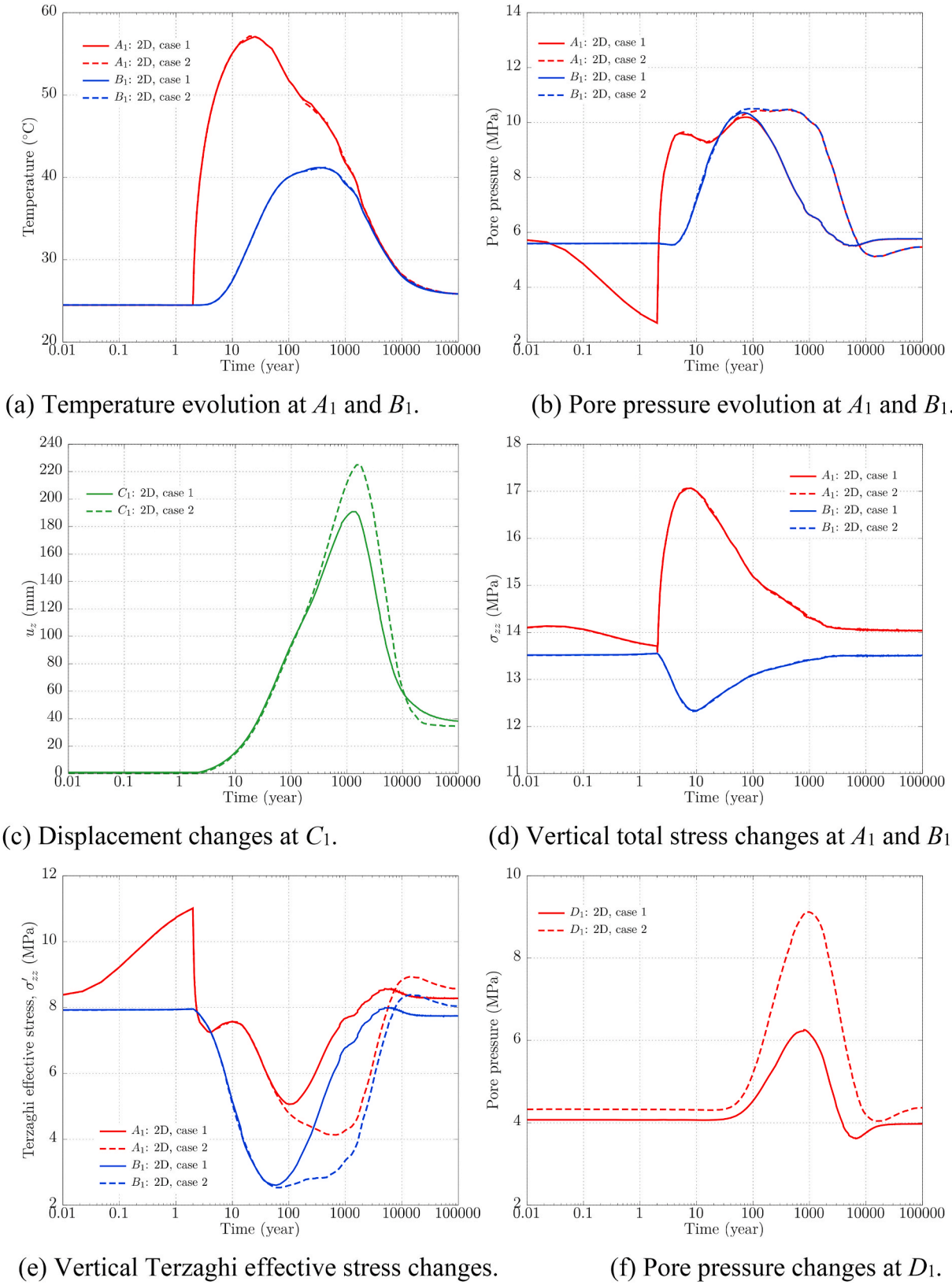

(a) Temperature evolution at A_1 and B_1.

(b) Pore pressure evolution at A_1 and B_1.

(c) Displacement changes at C_1.

(d) Vertical total stress changes at A_1 and B_1.

(e) Vertical Terzaghi effective stress changes.

(f) Pore pressure changes at D_1.

Fig. 11. 2D THM simulation results with different permeability for comparison.

Overall, the study shows the importance of the repository-scale host-rock temperature evolution which can be the limiting factor in thermal management of a nuclear waste repository in argillaceous claystone. Future work will include modeling of hydro-fracturing induced by a temperature shock and thermal pressurization in COx claystone at the MHM URL. The work will be part of the new DECOVALEX-2023 project.[13]

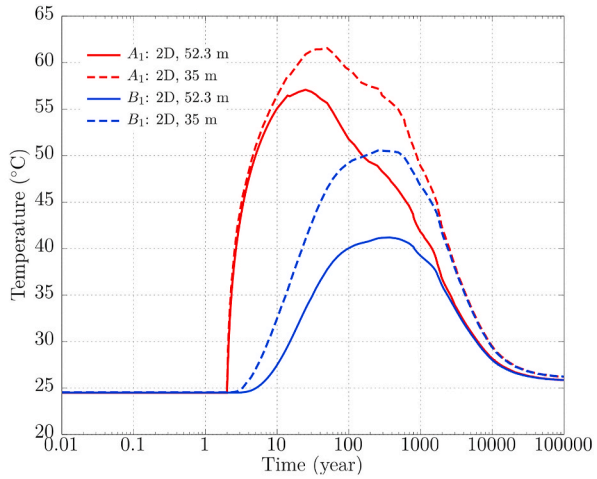

(a) Temperature evolution at A_1 and B_1.

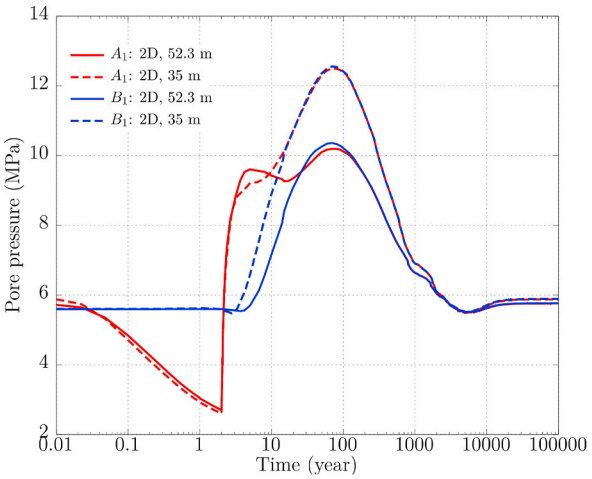

(b) Pore pressure evolution at A_1 and B_1.

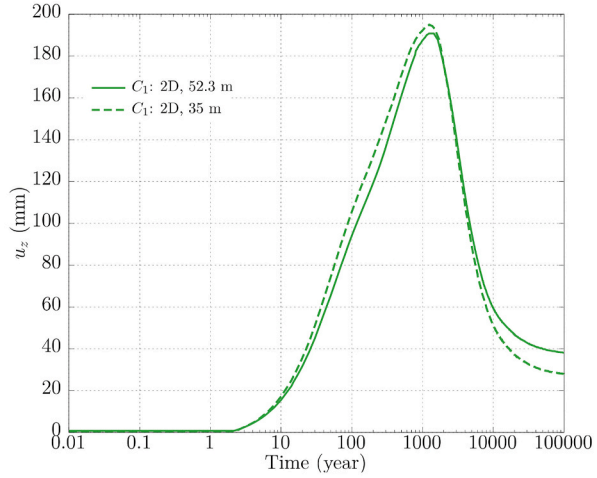

(c) Displacement changes at C_1.

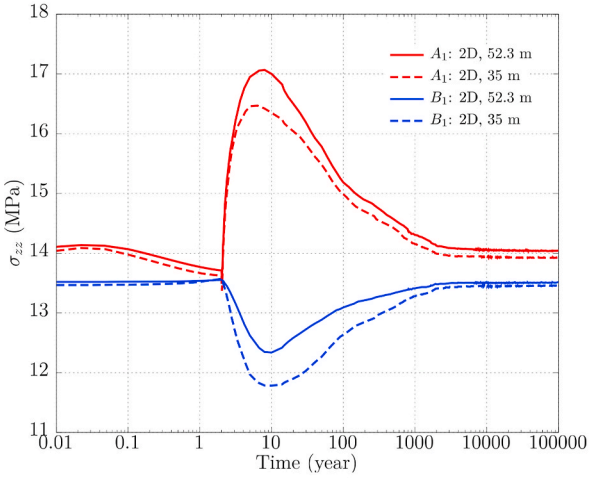

(d) Vertical total stress changes at A_1 and B_1.

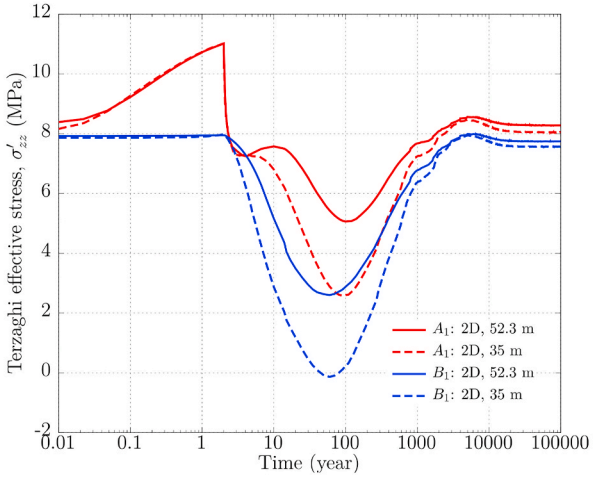

(e) Vertical Terzaghi effective stress changes at A_1 and B_1.

Fig. 12. 2D THM simulation results with different cell spacings for comparison.

Declaration of competing interest

The authors declare that they have no known competing financial interests or personal relationships that could have appeared to influence the work reported in this paper.

Acknowledgments

DECOVALEX is an international research project comprising participants from industry, government and academia, focusing on development of understanding, models and codes in complex coupled problems in sub-surface geological and engineering applications; DECOVALEX-2019 is the current phase of the project. The authors appreciate and thank the DECOVALEX-2019 Funding Organizations ANDRA, BGR/UFZ, CNSC, US DOE, ENSI, JAEA, IRSN, KAERI, NWMO, RWM, SÚRAO, SSM and Taipower for their financial and technical support of the work described in this paper. Funding for LBNL's modeling work was provided by the Spent Fuel and Waste Science and Technology, Office of Nuclear Energy, of the U.S. Department of Energy under Contract Number DE-AC02-05CH11231 with Lawrence Berkeley National Laboratory. The statements made in the paper are, however, solely those of the authors and do not necessarily reflect those of the Funding Organizations.

References

1 Conil N, Armand G, De La Vaissiere R, et al. In situ heating test in Callovo-Oxfordian clay-stone: measurement and interpretation. In: *Clays in Natural and Engineered Barriers for Radioactive Waste Confinement*. 2012.
2 Armand G, Bumbieler F, Conil N, de la Vaissière R, Bosgiraud J-M, Vu M-N. Main outcomes from in situ thermo-hydro-mechanical experiments programme to demonstrate feasibility of radioactive high-level waste disposal in the Callovo-Oxfordian claystone. *Journal of Rock Mechanics and Geotechnical Engineering*. 2017;9(3):415–427. https://doi.org/10.1016/j.jrmge.2017.03.004.
3 François B, Laloui L, Laurent C. Thermo-hydro-mechanical simulation of ATLAS in situ large scale test in Boom Clay. *Comput Geotech*. 2009;36(4):626–640. https://doi.org/10.1016/j.compgeo.2008.09.004.
4 Chen G, Sillen X, Verstricht J, Li X. ATLAS III in situ heating test in boom clay: field data, observation and interpretation. *Comput Geotech*. 2011;38(5):683–696. https://doi.org/10.1016/j.compgeo.2011.04.001.
5 Gens A, Vaunat J, Garitte B, Wileveau Y. In situ behavior of a stiff layered clay subject to thermal loading: observations and interpretation. *Geotechnique*. 2007;57(2):207–228. https://doi.org/10.1680/geot.2007.57.2.207.
6 Garitte B, Nguyen TS, Barnichon JD, et al. Modelling the Mont Terri HE-D experiment for the Thermal–Hydraulic–Mechanical response of a bedded argillaceous formation to heating. *Environmental Earth Sciences*. 2017;76(9):345. https://doi.org/10.1007/s12665-017-6662-1.
7 Hansen FD, Hardin EL, Rechard RP, et al. *Shale Disposal of U.S. High-Level Radioactive Waste, SAND2010-2843*. Albuquerque, New Mexico: Sandia National Laboratories; 2010.
8 Hendry MJ, Solomon DK, Person M, et al. Can argillaceous formations isolate nuclear waste? Insights from isotopic, noble gas, and geochemical profiles. *Geofluids*. 2015;15:381–386. https://doi.org/10.1111/gfl.12132.
9 Rutqvist J, Zheng L, Chen F, Liu H, Birkholzer J. Modeling of coupled thermo-hydro-mechanical processes with links to geochemistry associated with bentonite-backfilled repository tunnels in clay formations. *Rock Mech Rock Eng*. 2014;47(1):167–186. https://doi.org/10.1007/s00603-013-0375-x.
10 Muñoz J, Alonso EE, Lloret A. Thermo-hydraulic characterization of soft rock by means of heating pulse tests. *Geotechnique*. 2009;59(4):293–306. https://doi.org/10.1680/geot.2009.59.4.293.
11 Ghabezloo S, Sulem J. Temperature induced pore fluid pressurization in geomaterials. *Italian Geotechnical Journal*. 2010;29–43.
12 Berchenko I, Detournay E, Chandler N. Propagation of natural hydraulic fractures. *Int J Rock Mech Min Sci*. 1997;34(3–4):63. https://doi.org/10.1016/S1365-1609(97)00189-5. e1–63.e11.
13 Birkholzer JT, Tsang C-F, Bond AE, Hudson JA, Jing L, Stephansson O. 25 years of DECOVALEX - scientific advances and lessons learned from an international research collaboration in coupled subsurface processes. *Int J Rock Mech Min Sci*. 2019;122:103995. https://doi.org/10.1016/j.ijrmms.2019.03.015.
14 Seyedi D, Plúa C, Vitel M, et al. Upscaling THM modelling from small-scale to full-scale in-situ experiments in the Callovo-Oxfordian claystone. *Int J Rock Mech Min Sci*. 2020. submitted.
15 Plúa C, Vu M, Armand G, et al. A reliable numerical analysis for large-scale modelling of a high-level radioactive waste repository in the Callovo-Oxfordian claystone. *Int J Rock Mech Min Sci*. 2020. submitted.
16 Xu H, Rutqvist J, Plúa C, Armand G, Birkholzer J. Modeling of thermal pressurization in tight claystone using sequential THM coupling: benchmarking and validation against in-situ heating experiments in COx claystone. *Tunn Undergr Space Technol*. 2020;103:103428. https://doi.org/10.1016/j.tust.2020.103428.
17 P. Lebon, B. Mouroux, B. Faucher, Status of Research on Geological Disposal of High-Level and Long-Lived Radioactive Waste in France. In P.A. Witherspoon and G.S Bodvarsson (editors), Geological Challenges in Radioactive Waste Isolation, Fourth Worldwide Review, 2006, Lawrence Berkeley National Laboratory, Berkeley, California, pp. 85–96. LBNL-59808, URL: https://eesa.lbl.gov/worldwide-review/..
18 Nguyen TS, Börgesson L, Chijimatsu M, et al. A case study on the influence of THM coupling on the near field safety of a spent fuel repository in sparsely fractured granite. *Environ Geol*. 2009;57:1239–1254. https://doi.org/10.1007/s00254-008-1565-9.
19 Rutqvist J, Barr D, Birkholzer JT, et al. A comparative simulation study of coupled THM processes and their effect on fractured rock permeability around nuclear waste repositories. *Environ Geol*. 2009;57:1347–1360. https://doi.org/10.1007/s00254-008-1552-1.
20 Rutqvist J. An overview of TOUGH-based geomechanics models. *Comput Geosci*. 2017;108:56–63. https://doi.org/10.1016/j.cageo.2016.09.007.
21 Pruess K, Oldenburg C, Moridis G. *TOUGH2 User's Guide, Version 2.1, LBNL-43134 (Revised)*. Berkeley, California: Lawrence Berkeley National Laboratory; 2012.
22 Itasca. *FLAC3D v5.0, Fast Lagrangian Analysis of Continua in 3 Dimensions, User's Guide*. Minneapolis, Minnesota: Itasca Consulting Group; 2011.
23 Kim J, Tchelepi HA, Juanes R. Stability and convergence of sequential methods for coupled flow and geomechanics: fixed-stress and fixed-strain splits. *Comput Methods Appl Mech Eng*. 2011;200(13):1591–1606. https://doi.org/10.1016/j.cma.2010.12.022.
24 Delay J, Vinsot A, Krieguer JM, Rebours H, Armand G. Making of the underground scientific experimental programme at the Meuse/Haute-Marne underground research laboratory, northeastern France. *Phys Chem Earth*. 2007;32(1/7):2–18.
25 Conil N, Manon V, Plúa C, Vu MN, Seyedi D, Armand G. In situ investigation of the THM behavior of the callovo-oxfordian claystone. *Rock Mech Rock Eng*. 2020;53:2747–2769. https://doi.org/10.1007/s00603-020-02073-8.
26 International Formulation Committee. *A Formulation of the Thermodynamic Properties of Ordinary Water Substance*. Düsseldorf, Germany: IFC Secretariat; 1967.
27 Rutqvist J, Graupner B, Guglielmi Y, et al. An international model comparison study of controlled fault activation experiments in argillaceous claystone at the Mont Terri Laboratory. *Int J Rock Mech Min Sci*. 2020;136, 104505. https://doi.org/10.1016/j.ijrmms.2020.104505.
28 Rutqvist J. Thermal management associated with geologic disposal of large spent nuclear fuel canisters in tunnels with thermally engineered backfill. *Tunn Undergr Space Technol*. 2020;102:103454. https://doi.org/10.1016/j.tust.2020.103454.
29 Zhang C-L, Conil N, Armand G. Thermal effects on clay rocks for deep disposal of high-level radioactive waste. *Journal of Rock Mechanics and Geotechnical Engineering*. 2017;9(3):463–478. https://doi.org/10.1016/j.jrmge.2016.08.006.
30 Blümling P, Bernier F, Lebon P, Martin CD. The excavation damaged zone in clay formations time-dependent behaviour and influence on performance assessment. *Phys Chem Earth, Parts A/B/C*. 2007;32(8-14):588–599. https://doi.org/10.1016/j.pce.2006.04.034.